Article

Treatment of Direct Red 28 Dye through *Phoenix dactylifera* L. Fruit Seed Biochar: Equilibrium, Kinetics, Thermodynamics, and Phytotoxicity Studies

Riti Thapar Kapoor [1,*], Mohd Rafatullah [2,3,*], Husnul Azan Tajarudin [3,4], Masoom Raza Siddiqui [5] and Mahboob Alam [6]

1   Centre for Plant and Environmental Biotechnology, Amity Institute of Biotechnology,
    Amity University Uttar Pradesh, Noida 201 313, Uttar Pradesh, India
2   Environmental Technology Division, School of Industrial Technology, Universiti Sains Malaysia,
    Gelugor 11800, Penang, Malaysia
3   Renewable Biomass Transformation Cluster, School of Industrial Technology, Universiti Sains Malaysia,
    Gelugor 11800, Penang, Malaysia; azan@usm.my
4   Bioprocess Technology Division, School of Industrial Technology, Universiti Sains Malaysia,
    Gelugor 11800, Penang, Malaysia
5   Chemistry Department, College of Science, King Saud University, Riyadh 11451, Saudi Arabia;
    mrsiddiqui@ksu.edu.sa
6   Division of Chemistry and Biotechnology, Dongguk University, 123, Dongdaero,
    Gyeongju-si 780714, Republic of Korea; mahboobchem@gmail.com
*   Correspondence: rkapoor@amity.edu (R.T.K.); mrafatullah@usm.my (M.R.)

Abstract: Wastewater discharge into aquatic systems has become a severe threat to the ecosystem. Herein, Direct Red 28 (DR28) dye removal from an aqueous solution was executed with the application of date fruit seed biochar (DFSB). Fourier transform infrared spectra (FTIR) and scanning electron microscopy (SEM) were utilized for the identification of functional groups and characteristics of the DFSB surface. A series of batch investigations were conducted to analyze pH, contact duration, biochar amount, dye concentration, temperature, and agitation speed on DR28 dye elimination from an aqueous medium by DFSB. The highest dye elimination, 97%, was recorded at a pH of 3 by DFSB at 250 mg/L DR28 dye concentration. The equilibrium data indicated the best fit with the Langmuir isotherm with $R^2 = 0.99$, showing 5.83 mg/g monolayer DR28 uptake potential. The best correlation coefficient of the sorption procedure was observed with a pseudo-second-order kinetic study. Investigations on thermodynamic variables disclosed favorable, impetuous exothermic processes. The sorption process was spontaneous as well as exothermic, which was reflected by analyses of thermodynamic parameters. DFSB showed a 33% DR28 dye adsorption ability for up to five successive cycles. DFSB-treated DR28 dye solution increased seedling growth and biochemical components of pigeon pea. The results of the present investigation revealed the significant capacity of DFSB for DR28 dye elimination. Date fruit seed biochar can be applied as an environmentally benign, sustainable adsorbent for DR28 dye removal from industrial effluent, as it is available at zero cost and converts wastewater into reusable biomaterial. Thus, the application of DFSB can assist in wastewater treatment, carbon sequestration, and waste management for a sustainable future.

Keywords: biochar; date fruit seed; direct red 28; wastewater; phytotoxicity

1. Introduction

Water is the most essential substance for the survival of all living beings. The expansion of industrial and anthropogenic activities, urbanization, and overpopulation enhance the discharge of industrial effluents into the environment. Dyes are toxic, colored, aromatic organic contaminants that are consumed in various industries, like paint, paper, textile, printing, cosmetics, and plastics [1–3]. The global dye market was around thirty-three

billion dollars in 2019 and may increase to 49 billion dollars by the year 2027 [4]. Approximately seventy million tons of synthetic coloring materials are generated annually for textile manufacturing units at the global level, and around 10–15% of dyestuff is not fixed in fabric and is discharged into wastewater during processing [5]. Textile industries generate employment opportunities and assist in the development of the national economy. Textile industries consume two hundred liters of water in the production of one kilogram of fabric and release large amounts of wastewater during the dyeing process [6]. However, industries discharge a huge amount of untreated dye-contaminated wastewater into the environment [7]. As per a World Bank report, 17–20% of total industrial pollution is due to textile industries [8]. The composition of textile industry effluent is complex, containing some amount of sulfur, which can be degraded to sulfide ions in the absence of oxygen and may release H_2S, which pollutes the environment [9]. The presence of dye in water at a lower amount makes it aesthetically and environmentally objectionable [10]. The high turbidity and dark color of dye-contaminated industrial effluent inhibits photosynthesis by decreasing the transmission of sunlight through water and also reduces dissolved oxygen level, resulting anoxic conditions with high BOD and COD [11]. The continuous release of recalcitrant compounds in the ecosystem has negative impacts on aquatic flora and fauna and serious consequences on human health, animals, and the plant ecosystem via the food chain [12].

Many synthetic dyes and their intermediates, like aromatic amines, are toxic, mutagenic, and carcinogenic [13]. Organically bound chlorine, a well-known carcinogen, is present in >40% of dyes [4]. Dye-contaminated wastewater can induce asthma, respiratory ailments, irritation of the skin, mental confusion, tuberculosis, heart disease, cancer, gene mutations, etc. [14,15]. Vadivel et al. [16] reported that approximately USD 1 billion is required to treat 640,000,000 m^3 of dye-contaminated wastewater annually. Various methods, like flocculation, membrane filtration, reverse osmosis, coagulation, precipitation, ion exchange, nanofiltration, photocatalytic degradation, ozonation, and Fenton methods, have been applied for wastewater treatment [17–19]. Adsorption has been used for dye removal due to its high efficiency, simple design, flexibility, wide accessibility, safe handling, good stability, reusability, cost-effectiveness, and sludge-free cleaning operation [20]. Several commercial adsorbents, like zeolite, graphene, chitosan, silica gel, resin, and activated carbon, have been utilized for the treatment of effluents [21].

The agriculture sector produces waste biomass in huge amounts, which can play a pivotal role in the circular economy [22]. Improper disposal of crop residues and burning lead to the generation of greenhouse gases, such as carbon dioxide, nitrous oxide, and methane; deplete soil nutrients and microbial populations; and pose serious threats to the environment and the health of human beings [23]. Biochar, an amorphous carbonaceous material showing high-stability tunable chemistry in multiple intricate environments, is produced by the thermochemical transformation of waste biomass at high temperatures under limited oxygen conditions and can be regenerated for multiple cycles [24]. The application of agricultural waste enhances environmental protection, carbon neutrality, and the recycling of natural resources and is available at zero cost [3,25]. In recent years, many studies have been conducted on the application of agro-waste biomass, like rice, coconut and barley husk, orange peel, sugarcane bagasse, groundnut, walnut and almond shells, and banana and pineapple peels, in industrial effluent treatment and dye removal due to their renewable texture, wide availability, high adsorption capacity, recyclability, and economic feasibility [15,26,27]. Biochar has been considered a supreme adsorbent due to its exceptional textural features, like its large surface area, porosity, chemical stability, high mechanical strength, enriched surface functional groups, and regenerative ability for pollutant removal [28–30]. Biochar materials are sustainable and better than conventional and commercially available carbon substances, and they can be used for sensing, electrocatalysis, and energy storage [31].

Direct red 28, an anionic diazo dye, has two azo chromophores and acidic auxochromes connected to the structure of benzene [32]. It forms benzidine, a carcinogen, after the split-

ting of the azo group. Direct red 28 can cause skin and eye irritation, adverse impacts on respiratory and reproductive organs, and cancer etc. [33,34]. It shows cytotoxic, carcinogenic, and mutagenic effects and chromosomal errors in mammalian cells [35]. Direct red 28 inhibited the growth and chlorophyll content of *Lemna minor* [32]. Date palm (*Phoenix dactlifera* L.; Family: Arecaceae) magic trees are widely cultivated around the globe. Date fruits are rich in sugar, amino acids, protein, and lipids and contain minerals, vitamins, fiber, and antioxidants [36,37]. Date fruits contain minerals like potassium, calcium, magnesium, phosphorus iron, selenium, and zinc [38]. Many bioactive components, like carotenoids, phenolic acid, flavonoids, tocopherol, and sterols are also present in date fruits and function as nutraceuticals [37]. These bioactive compounds provide protection against inflammation, oxidative stress, and neurodegenerative disorders, such as Alzheimer's disease. Date seeds are an enormously produced agricultural waste that comprise around 11–18% of the date fruit's weight [39]. Pigeon pea (*Cajanus cajan* L. Millsp.; family: Fabaceae), also known as red gram, congo, or gungo pea, is widely grown in different parts of the world [40,41]. The seeds of *Cajanus cajan* are a rich source of protein, minerals, and fatty acids and are used for the treatment of diabetes and hepatitis due to the presence of bioactive compounds. The leaves of pigeon pea have antibacterial, anti-inflammatory, anticancer, antioxidant, and neuroprotective properties [41]. To the best of our knowledge, this is the first investigation to examine the effects of date fruit seed biochar on DR28 dye sorption and the further impact of treated DR28 dye solution on the growth and biochemical attributes of pigeon pea. The major objectives of this study were to synthesize biochar from date fruit seeds and characterize it, explore the sorption performance of DR28 using DFSB, and examine the sorption results for the applicability of various isotherm, kinetic, and thermodynamic variables. We also tested the reusability and feasibility of DFSB and assessed the reutilization of treated contaminated water on the growth, development, and biochemical processes of pigeon pea.

2. Materials and Methods

2.1. Date Fruit Seed Biochar Production

Date fruits were purchased from a local grocery store in Noida, Uttar Pradesh, India. Date seeds were cleansed with distilled water for dust removal and placed in the shade for up to ten days to decrease the water amount. The pyrolysis reactor was utilized for the production of biochar; nitrogen gas was given to the reactor to create an inactive atmosphere, and temperature was controlled. The seeds were ground and placed in the reactor for 4 h at 500 °C. The DFSB was crushed and cleansed with slightly warm deionized water and placed in an electric oven at 65 °C for 2 h to inhibit microbial activity [42]. Proximate examination was conducted to assess moisture, fixed carbon, ash, and volatile material in the DFSB under thermochemical modifications.

2.2. Materials and Preparation of Reagents

Direct Red 28, also known as Congo red, was procured from Merck, Mumbai. Seeds of pigeon pea (*Cajanus cajan* L. Millsp variety Prabhat) were procured from the seed agency of Noida. Different concentrations of Direct Red 28 dye solution were prepared with distilled water. Analytical-grade chemicals were used without purification. DR28 dye solution absorbance was taken with a spectrophotometer (Shimadzu 1800, Kyoto, Japan). Table 1 shows the dye characteristics.
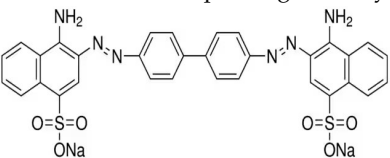
2.3. Batch Experiments

A batch study was conducted to analyze the feasibility of using DFSB for the removal of DR28 dye. The impact of different attributes, like pH (3–11), particle size (0–500 μm), contact time (60–360 min), doses of biochar (2–4.5 g), DR28 concentration (150–400 mg/L), temperature (30–55 °C), and agitation speed (50–300 rpm), were applied for DR28 dye removal from an aqueous medium with DFSB. One hundred milliliters of DR28 dye concentrations (150, 200, 250, 300, 350, and 400 mg/L) was kept in six different flasks, and

DFSB in amounts of 2, 2.5, 3, 3.5, 4 and 4.5 g were added, respectively. No DFSB was added to the DR28 dye solution in the control flasks. The DR28 dye concentration before and after DFSB addition was analyzed by UV–Vis spectrophotometer (λmax = 497 nm), and sorption efficiency was estimated by the following formula:

$$\text{Removal of DR28 dye} = (C_0 - C_t)/C_0 \times 100 \tag{1}$$

C_0 and C_t = initial and final concentration of DR28 (mg/L), respectively.

Table 1. Properties of Direct Red 28.

Stuff	Congo Red 4B, Cosmos Red, Direct Red Y
C.I. Number	11313
Color	Red-Brown
Type	Anionic dye
Melting point	>360 °C
Solubility	Water-soluble and less soluble in organic solvents
IUPAC name	disodium;4-amino-3-[[4-[4-[(1-amino-4-sulfonatonaphthalen-2-yl)diazenyl]phenyl]phenyl]diazenyl]naphthalene-1-sulfonate
Formula	$C_{32}H_{22}N_6Na_2O_6S_2$
Molecular weight	696.7 g mol^{-1}
Application	Used in textile and printing industry
Structure	
λmax	497 nm

2.4. Point Zero of Charge

Rivera-Utrilla et al.'s [43] procedure was used for the estimation of point zero of charge. A pH range of 3–11 for the NaCl solution (0.01 M) was maintained with 0.10 M hydrogen chloride and sodium hydroxide. DFSB (1 g) was incorporated in each solution and kept for 24 h at room temperature, and then pHfinal was measured. The pHPZC was estimated with the help of a graphical plot with the following formula:

$$\text{pH}_{final} - \text{pH}_{initial} = f\,(\text{pH}_{initial})$$

2.5. Characterization of Date Fruit Seed Biochar

The KBr pellet procedure was used for the identification of binding sites present on DFSB before and after DR28 dye adsorption with Fourier-transform infrared spectroscopy (Perkin Elmer 2000, Waltham, MA, USA). The DFSB surface was detected with SEM (Quanta FEG 650, Thermo Fisher, Beverly, CA, USA).

2.6. Adsorption Isotherm

For the determination of equilibrium adsorption, different isotherm models were applied. Direct Red 28 (250 mg/L) solution was taken with different DFSB amounts for the estimation of the isotherm feasibility by analyzing their uptake potential.

2.6.1. Langmuir Isotherm

This isotherm reflects that the energy of sorption was consistent on DR28 layer at DFSB surface at constant temperature [44]. It can be written as:

$$\frac{C_e}{q_e} = \frac{1}{q_m K_L} + \frac{C_e}{q_m} \tag{2}$$

where q_e = sorption of DR28 at equilibrium (mg g^{-1}), q_m = maximum DR28 sorption (mg g^{-1}), C_e = DR28 concentration at equilibrium (mg L^{-1}), and K_L = Langmuir constant related to the binding of DR28 on DFSB.

2.6.2. Freundlich Isotherm

It explains the dispensation of DR28 dye between DFSB and the solution at equilibrium. This reflects variation in active site energy augmentation for sorption and the decrease in sorption heat (Ng et al. [45]). It is described as:

$$\ln q_e = \ln K_F + \left(\frac{1}{n}\right)\ln C_e \tag{3}$$

where K_F = adsorption capacity and n = intensity, respectively. The adsorption procedure can be described as follows: $n < 1$ reflects chemisorption, $n > 1$ indicates physisorption, and $n = 1$ is linear adsorption.

2.6.3. Temkin Isotherm

It describes that the molecules' sorption heat in a layer decreases with dispersal due to the interactivity between DR28 and DFSB, and sorption reflects the constant dissemination of energies for binding to its maximum level.

The equation is given below as per the procedure of Temkin and Pyzhev [46]:

$$q_e = R_T/b_T \ln (A_T) + RT/b_T \ln (C_e) \tag{4}$$

where A_T = Temkin isotherm constant (L g^{-1}), b_T = Temkin constant for sorption heat (J mol^{-1}), R = gas constant (J/mol·K), and T = temperature.

2.7. Kinetics of Sorption Phenomenon

Modeling for sorption was conducted to assess the time for equilibrium and the rate for the adsorption process. Different models were applied for rate constant determination in the uptake procedure.

Lagergren's [47] method explained the pseudo-first-order mechanism as:

$$\ln (q_e - q_t) = \ln q_e - k_1 t \tag{5}$$

where q_e and q_t = DR28 dye sorption at equilibrium and time and k_1 = pseudo-first-order adsorption rate constant (min^{-1}).

This is explained by the following equation of Ho and Mckay [48]:

$$t/q_t = 1/k_2 \, q_e^2 + t/q_e \tag{6}$$

where q_e = DR28 sorption on DFSB at equilibrium and k_2 = the adsorption rate constant for pseudo-second-order (g/mg.min).

Molecules of DR28 dye were transported to the surface of DFSB from the dye solution and penetrated from the biochar surface to the subsequent phase; this is a moderate step in kinetics that determines rate. The intraparticle diffusion model of Weber and Morris [49] explains the association between q_t and $t^{1/2}$, as given below:

$$q_t = k_{diff} \, t^{1/2} + C \tag{7}$$

where k_{diff} = intraparticle diffusion rate constant (mg/g min$^{0.5}$), q_t = sorption capacity in time (mg g^{-1}), and C = thickness of the boundary layer.

2.8. Thermodynamics Parameters

The modifications in enthalpy, entropy, and free energy were determined for DR28 adsorption by DFSB. Different variables were assessed with the given equations:

$$\Delta G^0 = -RT \, \ln \, K_d \tag{8}$$

$$K_d = \frac{q_e}{C_e} \tag{9}$$

$$\Delta G^0 = \Delta H^0 - T\,\Delta S^0 \tag{10}$$

Modifications of ΔG, ΔS, and ΔH were assessed with the rearrangement of equations and the application of the curve-fitting process for the sorption mechanism.

2.9. Estimation of Reusability Capacity

Date fruit seed biochar (3 g) was added to a solution of DR28 dye (250 mg/L) and kept in a shaking incubator at 28 ± 2 °C at 200 rpm for up to 240 min. The optical density of the supernatant was measured after centrifugation to assess dye uptake by the biochar, and the DFSB-containing dye was separated. Samples without DFSB were used as a control to compare with samples containing DFSB for the removal of DR28 dye. DFSB with Direct Red 28 dye was placed at 50 °C for 6 h to increase the DFSB microstructure and dye uptake capacity. Date fruit seed biochar was rinsed with 1N hydrochloric acid and sodium hydroxide and placed at 180 rpm for up to 50 min, and the desorbing solution absorbance was measured [50]. The DFSB was separated, rinsed properly using distilled water to discard the desorbing solution, and placed for eight hours at 50 °C. DFSB viability was tested for 5 consecutive cycles. Desorption of DR28 was analyzed with the following formula:

Desorption (%) = DR28 dye content desorbed/DR28 dye adsorbed $\times$ 100 (11)

2.10. Assessment of Phytotoxicity

The effect of Direct Red 28 dye before and after DFSB treatment on the seeds of pigeon pea was assessed. Seeds of pigeon pea were cleaned with distilled water; then, 10% sodium hypochlorite was used for five minutes for surface treatment to arrest microbial activity, after that seeds were further rinsed with Milli-Q water. In the seed germination test, ten pigeon pea seeds were placed in different test tubes in distilled water, DR28 dye (250 mg/L), and DFSB-treated DR28 dye solution for five hours. Then, the seeds of pigeon pea were shifted to autoclaved Petri dishes in a seed germinator at 87% humidity and 27 ± 2 °C for a 12 h photoperiod for two weeks. For the estimation of germination, seedling length, fresh and dry weight, and vigor index, the ISTA [51] procedure was applied.

Germination (%) = Pigeon pea seeds germinated/pigeon pea seeds kept for germination $\times$ 100

Vigor index (VI) = Length of seedling $\times$ germination (%)

2.11. Analyses of Biochemical Constituents

Pigment components were analyzed as described by Lichtenthaler [52]. The contents of sugar, proline, and protein were assessed in pigeon pea with the procedures of Hedge and Hofreiter [53], Bates et al. [54], and Lowry et al. [55], respectively.

2.12. Statistical Analysis

All the treatments were organized with 3 replicates in a randomized block design. ANOVA and SPSS were applied for the analyses of the results. The treatment mean was estimated by DMRT at $p < 0.05$.

3. Results and Discussion

Date fruit seeds are widely accessible in huge amounts and can be an economical and sustainable alternative to activated carbon for the treatment of dye-contaminated effluent. Date fruit seed biochar (DFSB) prepared from date fruit seed waste acts as a catalyst, as it interacts with DR28 dye molecules and catalyzes the reaction, and it has an inert nature toward other reagents during the adsorption of DR28 dye from an aqueous solution.

3.1. Proximate Analyses of Sorbent

Proximate assessment was conducted to analyze the moisture, volatile matter, ash, and fixed carbon in DFSB. During pyrolysis, the breakage of bonds in molecules takes place because of heat treatment with the release of gas and liquid leaving the material with a high carbon content. Fixed carbon refers to a high quality of adsorbent due to enhanced adsorption capacity and high surface area. The results revealed the highest amount of volatile matter and fixed carbon, whereas a lower amount of ash was recorded after proximate analysis (Table 2).

Table 2. Proximate analyses of DFSB.

S. No.	DFSB	Weight (%)
1.	Volatile matter	66.55
2.	Fixed carbon	25.20
3.	Moisture	5.50
4.	Ash	2.75

3.2. Characterization of Date Fruit Seed Biochar

The FTIR spectra of the DFSB from wavenumbers 500–4000 cm^{-1} are reflected in Figure 1. The broadest band at 3413 cm^{-1} showed the availability of hydroxyl groups. Because of the C-H stretching vibration of -CH$_3$, CH$_2$, and methoxy groups, the spectrum was recorded at 2922 cm^{-1}. The adsorption peak at 2847 cm^{-1} was associated with the C-H alkane functional group with weak intensity. The presence of carboxyl or carbonyl functional groups was related to the carboxylate anion 1642 cm^{-1} band of DFSB, which was considered responsible for the chelation of dye molecules in DFSB. The bands at 1429 and 1086 cm^{-1} reflected C-H bending and C-O-C stretching, respectively (Figure 1). The peaks at 1321 and 1367 cm^{-1} were due to the presence of alkane, carbonyl, and hydroxyl functional groups. The FTIR spectra reflected that -OH, C-O, and -COOH were the major functional groups of DFSB, which showed a promising function in DR28 dye uptake. Moreover, sorption at 778 cm^{-1} exhibited the C-Cl alkyl halide functional group on the surface of the biochar. Thus, the adsorbent structure and adsorption capacity were influenced by the availability of functional groups on DFSB [27].
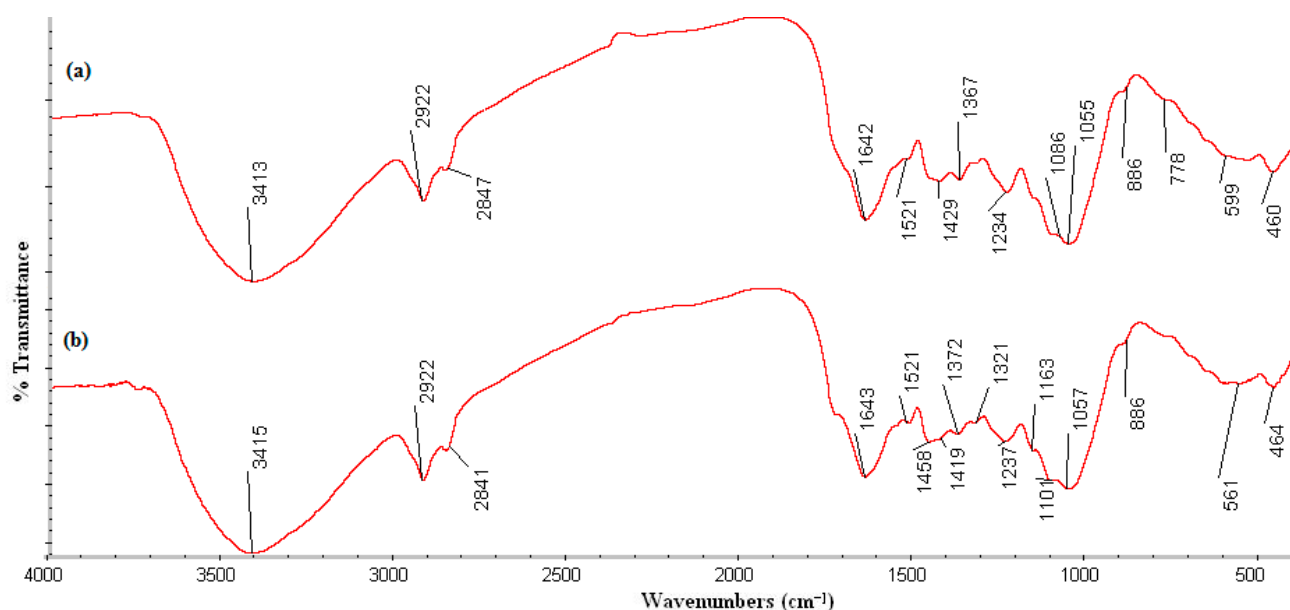

Figure 1. FTIR of DFSB (**a**) before and (**b**) after DR28 dye sorption.

After pyrolysis, scanning electron micrography was conducted to check for modifications in the structural morphology and the pores present in DFSB. The SEM micrograph

of the date fruit seed biochar before and after the sorption phenomenon was analyzed at a 15.00 KX magnification resolution with a 200 nm DFSB particle size. Remarkable alterations were observed in DFSB after the sorption of DR28 dye compared with biochar without dye (Figure 2). Due to organic matter volatilization in pyrolysis, channels with pores were clearly observed, as shown in Figure 2b [26]. A firmly bound surface was observed prior to sorption, while after DR28 dye sorption, a porous and heterogeneous structure was reflected due to chemical modifications of DFSB, as carboxyl, carbonyl, and hydroxyl groups were generated after lignin oxidation (Figure 2a). DR28 containing SEM images showed that active spaces were filled with dye molecules after DFSB interaction. Honeycomb-like porous structures were formed due to multi-layered carbon positioning, which exhibited aromatic moieties in DFSB with temperature enhancement (Figure 2b).
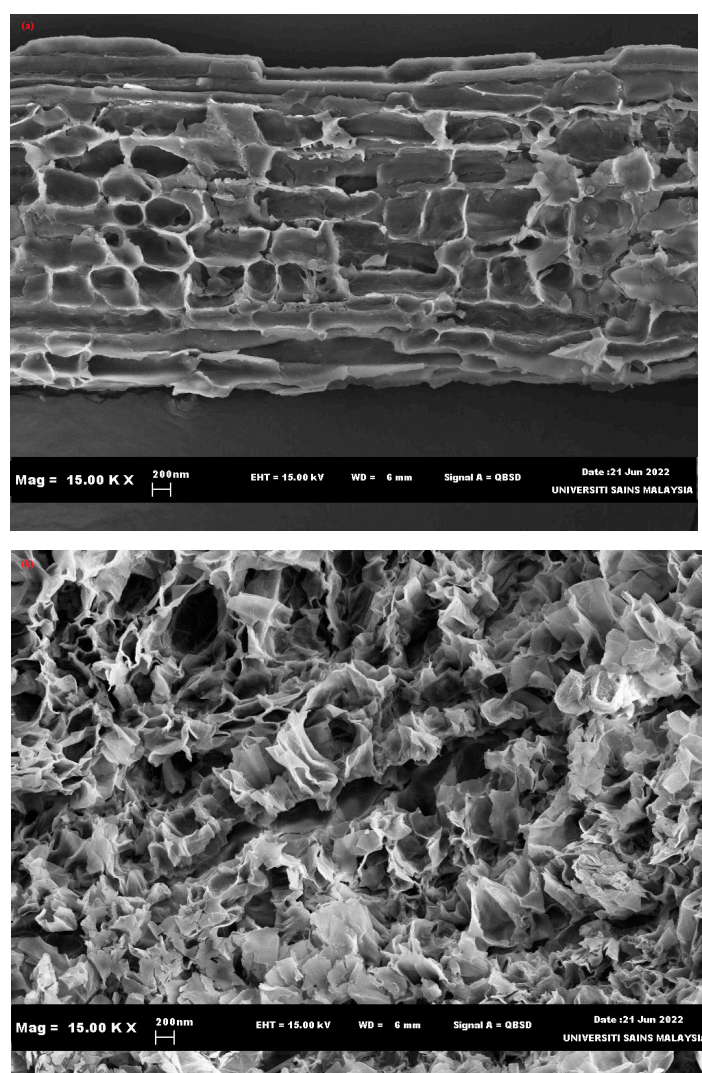

Figure 2. Scanning electron micrographs of DFSB adsorption procedure. (**a**) DFSB with spaces that can uptake DR28 dye and (**b**) pores with DR28 dye molecules.

3.3. Batch Experiments

The impact of different variables, like the pH, size of particles, contact period, dye concentration, biochar amount, speed of agitation, and temperature, were analyzed for DR28 dye elimination from the aqueous medium by DFSB. Additionally, the sorption efficacy of the phenomenon was analyzed by different isotherms and kinetic modeling.

3.3.1. Impact of pH

The pH of a solution is an important variable that affects dye solubility and the charge on the surface, dye speciation, ionization degree, and dye sequestration onto the adsorbent surface [56]. The pH affects the physicochemical properties of DFSB and changes the speciation of dye in the solution [57]. The effect of pH (3–11) on DR28 sorption (150–400 mg/L) on DFSB was examined at 25 ± 2 °C (Figure 1a). The highest DR28 sorption, 97%, was reported at a pH of 3, and pH values of 5, 7, 9, and 11 showed 89, 76, 58, and 42% DR28 dye elimination, respectively (Figure 3a). The electrostatic interplay between the negatively charged DR28 dye and the positively charged DFSB promoted DR28 dye attachment on DFSB. At a low pH, the concentration of H^+ ions was enhanced, which reduced the competition between hydroxyl ions and the dye and raised the DR28 dye sorption on the adsorbent surface [58]. The lower dye uptake at a high pH was due to OH^-, which competes for sorption spaces with other anions. The protonation of the DFSB surface was reduced, and negative charge generation exhibited electrostatic repulsion between the DR28 dye and DFSB with a rise in pH and decreased dye adsorption. The interaction between the dye and the biochar converted into Van der Waals pressure, which reflected less effect as compared to electrostatic attraction and ultimately reduced sorption. Similar findings were observed by Dai et al. [59]. They utilized crab shell biochar for DR28 dye removal at an acidic pH. Nautiyal et al. [60] recorded an 85–76% reduction in DR28 dye elimination by the biochar of *Spirulina platensis* when the initial pH was increased. Rehman et al. [61] reported 87% removal of DR28 dye at a pH of 3 with *Raphanus sativus* peel as a sorbent. Yang et al. [62] reported a reduction in DR28 dye removal with an increasing solution pH.

3.3.2. Particle Size

DR28 dye sorption was assessed with various sizes of DFSB particles: 0–170, 230–300, and 320–500 μm. With a reduction in DFSB particle size, DR28 dye sorption was enhanced due to the high surface area available on minute particles, which was proportional to the sorption of DR28 dye (Figure 3a). The diffusion barrier to mass transport was higher for large DFSB particles; the internal surface could not be utilized for sorption, and there was less uptake of DR28 dye.

3.3.3. Contact Period

The adsorption of dye at various contact periods and the time to reach sorption equilibrium are significant factors in the sorption process. Removal rates of DR28 dye (250 mg/L) of 62, 75, 84, and 93% were observed at 60, 120, 180, and 240 min, respectively. The DR28 dye adsorption was enhanced for up to 240 min; after this, a decrease was recorded (Figure 3b). Various unoccupied sites were available initially; with increase in time, DR28 dye attached to the available sites until these were filled, then dye uptake was checked. After 240 min, the uptake of DR28 dye was not enhanced, and this was considered the equilibrium time for the adsorption phenomenon (Figure 3b). The driving force of the concentration gradient was higher between DFSB and DR28 and the sorption rate was fast at the initial contact time. As time progressed, less uptake was recorded due to the absence of empty sorption sites or the enhanced repulsive forces between the DR28 sorbed on DFSB and the deprivation of concentration gradient pressure for the DR28 dye to combat mass movement obstruction to bind with DFSB [63].

3.3.4. Dose of Adsorbent

The DR28 dye removal rate depends on the amount of sorbent [64]. Date fruit seed biochar contains cellulose and lignin, which have active sites that bind with dye [65]. The impact of adsorbent doses (0.5–4.5 g) on DR28 dye removal is presented in Figure 3c. Direct Red 28 dye removal was enhanced from 69 to 94% with an increase in the DFSB dose (Figure 3c). The highestDR28 dye removal, 94%, was recorded with 3 g DFSB. With an increase in the sorbent amount, the surface area and number of active sites increased,

which improved the sorption capacity of the biochar [14]. However, with an increase in the biochar amount beyond the optimum level, the DR28 dye removal efficiency did not show significant changes. This might be due to compaction of adsorbent particles, formation of cluster between dye molecules and biochar, overlapping of binding sites which covered porous structure and made binding sites unavailable for sorption and dye removal efficiency was reduced [66].
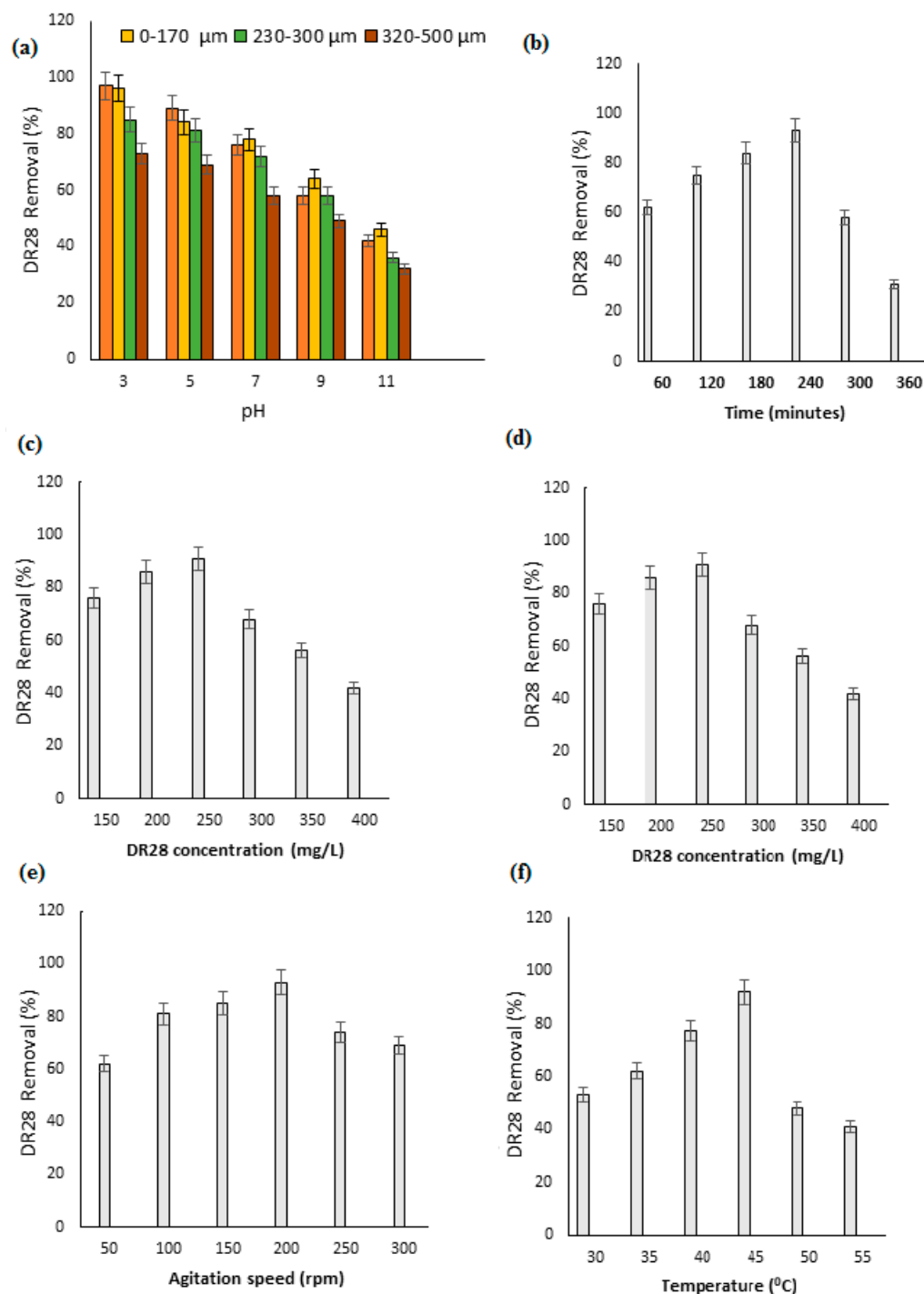

Figure 3. Effect of different variables—(**a**) pH and particle size, (**b**) contact period, (**c**) concentration of dye, (**d**) DFSB amount, (**e**) agitation speed, and (**f**) temperature—on DR28 dye (250 mg/L) removal by DFSB.

3.3.5. Concentration of Dye

The initial dye concentration in an aqueous medium acts as a driving force and regulates mass transfer resistance between the biochar and the dye. DR28 dye removal was increased with an increase in dye concentration; however, with a higher DR28 dye amount, the dye sorption rate was reduced (Figure 3d). The highest DR28 adsorption, 91%, was recorded with a 250 mg/L dye concentration. An increase in the initial dye concentration promotes the mass gradient between the dye solution and the biochar and creates driving pressure for DR28 molecule transfer from the solution to the biochar surface [67]. The concentration gradient could not pull the DR28 dye via the transmission barrier between DR28 and DFSB with a lower dye concentration, and active sites were available for dye sorption on DFSB; however, the findings were reversed with an increase in dye concentration. No dye molecules could attach to DFSB at a higher concentration, as the sorbent had few active sites that became saturated at the optimum concentration.

3.3.6. Agitation Speed

The removal of DR28 dye was enhanced with an increase in the speed of agitation, as reported in Figure 3e. Agitation speed enhancement decreased the boundary sheet barrier for DR28 dye movement from the solution to the DFSB [68]. With agitation speed enhancement, the interactivity between DR28 dye and DFSB particles was increased due to DFSB dispersion degree enhancement in the dye solution. The maximum agitation speed required more energy; no increase in DR28 dye elimination was reported at 250 and 300 rpm, and hence 200 rpm was regarded as the optimal agitation speed and showed 93% DR28 dye adsorption.

3.3.7. Temperature

Direct Red 28 dye adsorption on DFSB was observed at various temperatures, like 30, 35, 40, 45, 50, and 55 °C. Direct Red 28 exhibited 53, 62, and 77% sorption at 30, 35, and 40 °C respectively, and the highest uptake of DR28 dye, 92%, was recorded at 45 °C (Figure 3f). The removal of DR28 dye at a high temperature was due to a rise in the motion of dye molecules with the increase in temperature and the presence of active sites. At 50 and 55 °C, DR28 dye adsorption was decreased, and the reflected sorption phenomenon was kinetically maintained by an exothermic procedure. According to Ambaye et al. [69], with rise in the reaction temperature, the biochar surface area increased however, oxygen-carrying binding sites on the surface were reduced, Wu et al. [70] reported that after increasing the temperature from 65 to 85 °C, the surface area, porosity, and volume of pores in litchi peel biomass increased because the kinetic energy of the molecules increased with the rise in temperature, which promoted the dispersal of molecules onto the sorbent. Bao and Zhang [71] observed that an increase in temperature could show swelling in the adsorbent's internal structure and allow dye molecules to pierce the sorbent. These results were similar to those observed by Saleh Bashanaini [72], in which malachite green removal with shell seed biochar increased by up to 95% by increasing the temperature up to 50 °C.

3.3.8. Point of Zero Charge

At the point of zero charge, the net charge biochar surface became neutral in the dye solution, and this is important for the description of the adsorption mechanism. A graphical plot shows that pHpzc was 5.7 for date fruit seed biochar (Figure 4). The positive charge on the DFSB surface was reflected when pH < pHpzc, while pH > pH_{PZC} exhibited a negative charge on the surface of DFSB and fetched positively charged molecules of the dye. Therefore, the point of zero charge at 5.7 confirmed that DFSB can easily adsorb DR28 anionic dye, as the pH of the solution was less than that at the point of zero charge.
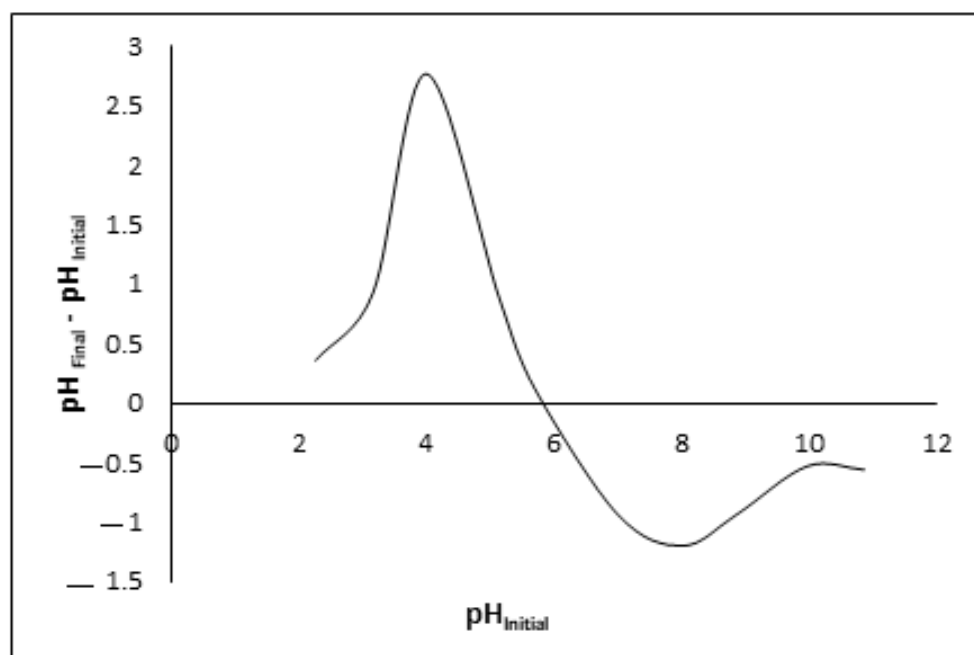
Figure 4. Graphical plot of point of zero charge of DFSB.

3.3.9. Equilibrium Modeling

Adsorption isotherms are mathematical associations that elucidate the nature of the interaction or competition between dyes and adsorbents, which assists in the understanding of the adsorption process [73]. The relationship between equilibrium data, either theoretical or practical, is needed for the elucidation of the extent of sorption. Langmuir, Freundlich, and Temkin isotherms were applied to examine the feasibility of DFSB applied for the sorption process. Equilibrium modeling explained the mechanism of sorption, the biochar surface properties, the uptake capacity of biochar, and the feasibility of the adsorption process (Table 3; Figure 5a–c). Direct Red 28 dye showed a homogenous monolayer covering DFSB. The Langmuir isotherm is based on the presumption that the adsorbent structure is homogeneous and all the active sites are similar. The sorption process cannot go beyond the monolayer, and every active site may a carry single dye molecule. The Freundlich isotherm deals with adsorption on heterogeneous surfaces, and adsorption increases with a rise in the concentration of dye. It has integrated interactions between the dye and the biochar surface.

Table 3. Isotherm constant for DR28 adsorption onto DFSB.

Isotherm	Equation	Variables	Value
Langmuir	$\frac{C_e}{q_e} = \frac{1}{q_m K_L} + \frac{C_e}{q_m}$	q_m (mg g^{-1}) K_L (l mg^{-1}) R^2	5.83 0.0021 0.9926
Freundlich	$\ln q_e = \ln K_F + \left(\frac{1}{n}\right)\ln C_e$	n K_F (mg g^{-1}) R^2	1.9120 1.0369 0.9147
Temkin	$q_e = R_T/b_T \ln(A_T) + R_T/b_T$ $\ln(Ce)$	b_T (J mole^{-1}) A_T (L mole^{-1}) R^2	4.0374 1.03552 0.9323

The Langmuir isotherm had the best fit in comparison with Freundlich and Temkin and reflected a high value of R^2 = 0.9926. It depicted a monolayer covering of DR28 on DFSB. The Langmuir constants showed the following parameters: q_m= 5.83 mg g^{-1} and k = 0.0021 mg^{-1}; the constants of Freundlich were K_f = 1.0369 and n = 1.9120, with

R^2 = 0.9147, and the Temkin constants were b_T = 4.0374 (J mole^{-1}) and A_T = 1.03552 (L mole^{-1}) with R^2 = 0.9323.
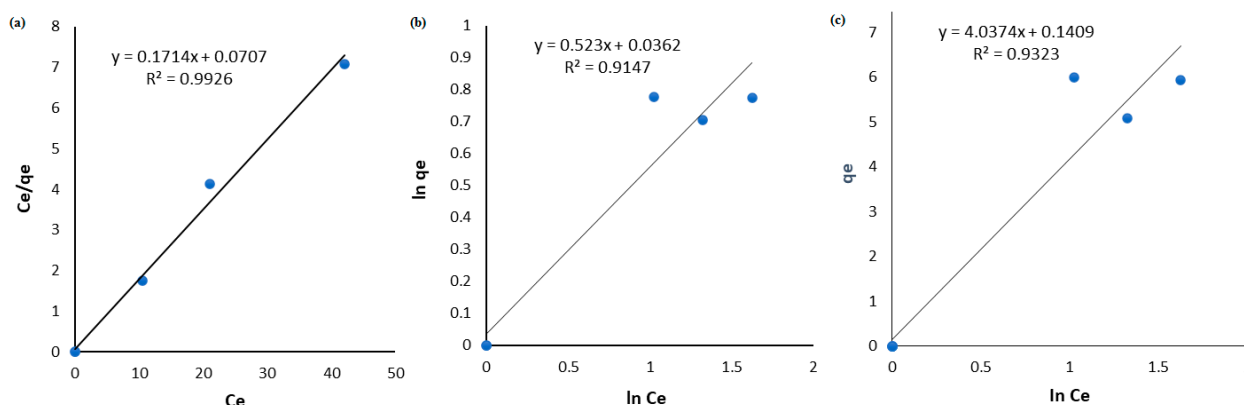

Figure 5. (**a**) Langmuir, (**b**) Freundlich, (**c**) and Temkin isotherms for DR28 dye adsorption on DFSB.

3.3.10. Kinetics of Adsorption

A kinetic study was applied to explain the sorption rate and adsorption process mechanism. The dye uptake mechanism was studied with various models. These models were used to determine the uptake of DR28 dye by DFSB to explain the reaction mechanism and sorption capacity. The kinetic equations were applied to observe the sorption process mechanism.

Pseudo-first-order, pseudo-second-order, and Weber–Morris intraparticle diffusion models were used to explain the kinetics of the sorption process (Table 4 and Figure 6a–c). Because of the low value of R^2, the difference in the results of the experiments, and the calculated equilibrium adsorption, the pseudo-first-order(R^2 = 0.1569) and Weber-Morris intraparticle diffusion (R^2 = 0.769) models could not explain the sorption process kinetics. The pseudo-second-order model had a higher value of R^2 = 0.8685, reflected correlation with the kinetics results, and described chemical interactions between the DR28 dye and DFSB [74].

Table 4. Application of kinetic model for DR28 dye sorption on DFSB.

Model	Equation	Variables	Value
Pseudo first order	$\ln(q_e - q_t) = \ln q_e - k_1 t$	$1K_1$ (min^{-1}) q_e (mg g^{-1}) R^2	0.0029 2.41042 0.1569
Pseudo second order	$\frac{t}{q_t} = \frac{1}{k_2 q_e} + \frac{t}{q_e}$	K_2 (g mg^{-1} min^{-1}) q_e (mg g^{-1}) R^2	0.00144 6.7159 0.8685
Weber–Morris intraparticle diffusion	$q_t = k_{diff}\, t^{1/2} + C$	K_{diff} C R^2	0.0273 1.6855 0.769

3.3.11. Thermodynamic Analysis

The effect of sorption temperature on DR28 removal capacity was assessed by thermodynamic parameters. The ΔG°, ΔH°, and ΔS° were used to analyze the adsorption phenomenon (Table 5). An adsorption study was conducted at various temperatures, i.e., 30 to 55 °C (Table 5). The dye adsorption feature was recognized by ΔH° [75]. The DR28 dye sorption on DFSB was a spontaneous and viable process, and it was clearly observed with a negative value of ΔG° [76]. The ΔG° value, reflecting the change in Gibbs free energy, was negative across various temperatures. A positive value of ΔS° (90.752 J/K) showed an increase in the adsorbate content in solid state. Furthermore, the positive entropy value

showed more randomness at the interface between the solid and solution during the sorption process. Positive entropy of adsorption signifies the attraction of DFSB to DR28 dye. The free energy was enhanced with an increase in the temperature of the sorption process, showing that a rise in temperature increased DR28 dye sorption.
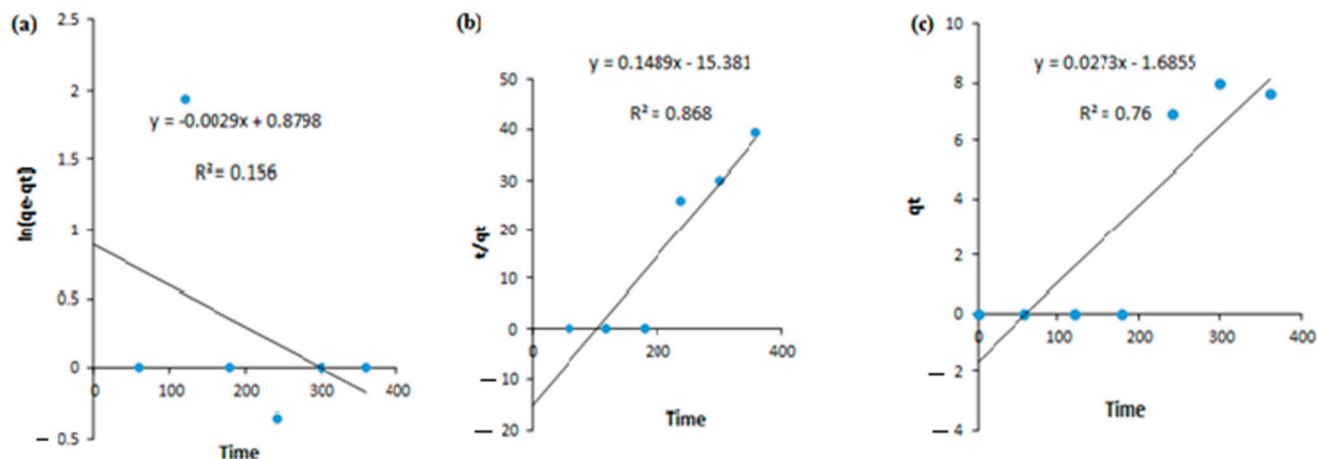

Figure 6. (**a**) Pseudofirst-order, (**b**) pseudo-second-order, and (**c**) Weber–Morris intraparticle diffusion models for DR28 sorption onto DFSB.

Table 5. Thermodynamic variables for sorption of DR28 dye with DFSB.

S. No.	Temperature (°C)	($\Delta G°$) (kJ mol^{-1})	$\Delta H°$ (kJ mol^{-1})	$\Delta S°$ (J K^{-1})
1.	30	−5377.67		
2.	35	−4976.33		
3.	40	−3822.26	−31.889	90.752
4.	45	−1388.72		
5.	50	−2361.86		
6.	55	−4256.75		

Entropy and enthalpy values were calculated by the plot between the natural log of kd and 1/T, $\Delta H°$ (−31.889 kJ/mol) and reflected an exothermic behavior of phenomenon. $\Delta S°$ (90.752 J K^{-1}) showed a positive value because of an increase in the DR28 concentration on DFSB in comparison with the dye solution [10]. The $\Delta S°$ value was positive at the DR28 and DFSB interface and reflected an increase in the degree of randomness.

3.3.12. Regeneration Analysis

The reusability of an adsorbent is a significant marker to analyze practical applications of the sorbent. The sorbent needs recyclability to achieve its maximum reutilization, in addition to its high sorption capacity. Recycling sorbents can reduce expenditure in the sorption process and energy consumption to provide sustainable products and restrict secondary pollution. Acidic and alkaline media were applied to remove DR28 from DFSB, as both positive and negative active sites were present in the dye solution. In the acidic medium, the dye solution consisted of H$^+$ that attached to the dye molecules with negative functional groups and desorbed from the adsorbent surface, whereas in an alkaline medium, dye molecules containing positive functional groups were removed. The regenerated DFSB showed 87, 75, 58, 45, and 33% dye sorption capacity for five cycles, respectively (Figure 7). However, there was a significant decrease in the sorption ability after the third cycle, which might have been due to the blockage of adsorption sites present in the DFSB micropores. Hence, used DFSB can be successfully used for DR28 dye removal.
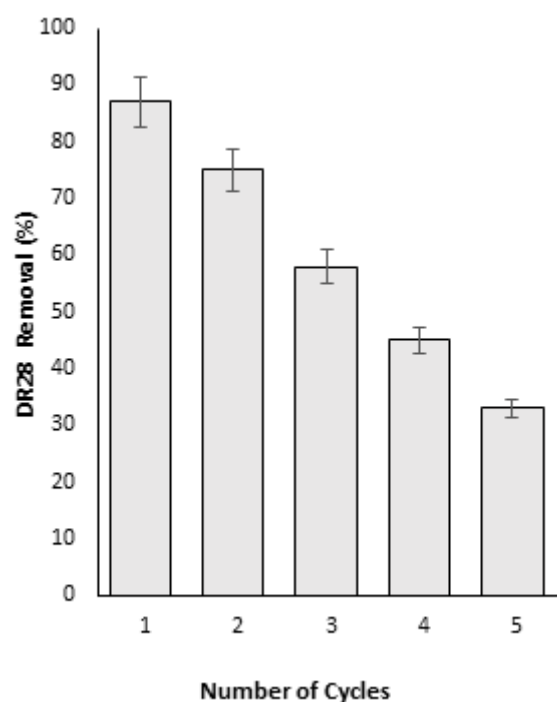
Figure 7. Removal of Direct Red 28 dye by DFSB for up to five consecutive cycles.

3.3.13. Evaluation of Phytotoxic Effects

The effect of Direct Red 28 dye on growth and physiological attributes of *Cajanus cajan* L. Millsp. var. Prabhat was assessed before as well as after DFSB treatment. The study was executed in different sets, i.e., the distilled water in the control, DR28 dye solution (250 mg/L), and DFSB-treated DR28 dye solution were applied in the second and third sets, respectively, for pigeon pea seed irrigation. The highest percentage of pigeon pea seeds, 98%, germinated in the control, whereas 12% germination was recorded after the use of DR28 dye solution (250 mg/L). Pigeon pea seeds reflected 83% germination with DFSB-treated DR28 dye solution. After two weeks, the seedling length, vigor index, and biochemical components were analyzed. The radicle and plumule length were 3.65 and 10.21 cm in the control and decreased to 0.87 and 2.75 with DR28 dye. The length and vigor index of the seedlings exhibited the following trend: control (distilled water) > DFSB-treated DR28 dye solution > DR28 dye solution (Table 6). *Cajanus cajan* seedlings showed the highest pigment, sugar, and protein amount in the control. Direct Red 28 dye solution showed 67, 71, and 79% reduction in total chlorophyll, sugar, and protein contents, respectively, in pigeon pea as compared to their control. The reduction in biochemical components was because of the negative impact of DR28 on the physiological attributes of pigeon pea plants (Table 7). However, the DFSB-treated DR28 dye solution enhanced the growth parameters of pigeon pea more than the DR28 dye solution.

Table 6. Impact of DR28 dye on the growth of *Cajanus cajan* L. Millsp. var. Prabhat.

Treatment	Germination (%)	Radicle Length (cm)	Plumule Length (cm)	Vigour Index
Control	98 ± 0.56 [a]	3.65 ± 0.15 [a]	10.21 ± 0.71 [a]	13,582.8
DR28 dye solution (250 mg/L)	12 ± 0.33 [c]	0.87 ± 0.01 [c]	2.75 ± 0.10 [c]	434.4
DFSB treated DR28 dye solution	83 ± 0.67 [b]	1.94 ± 0.03 [b]	8.10 ± 0. 34 [b]	8333.2

Data presented are means ± SD (n = 3). Different letters after the values indicate significant variation between treatments at $p < 0.05$ significance level as per ANOVA.

Table 7. Impact of DR28 dye on biochemical components of *Cajanus cajan* L. Millsp. var. Prabhat.

Treatment	Chlorophyll (mg g^{-1} FW)	Sugar (mg g^{-1} DW)	Protein (mg g^{-1} FW)
Control	2.89 ± 0.05 [a]	3.95 ± 0.09 [a]	24.12 ± 0.05 [a]
DR28 dye solution (250 mg/L)	0.94 ± 0.02 [c]	1.15 ± 0.22 [c]	5.11 ± 0.38 [c]
DFSB treated DR28 dye solution	1.67 ± 0.06 [b]	2.42 ± 0.08 [b]	16.09 ± 0.43 [b]

Data presented are means ± SD (n = 3). Different letters after the values reflect significant variation between treatments at $p < 0.05$ significance level as per ANOVA.

3.3.14. Performance of Date Fruit Seed Biochar

The DR28 dye adsorption ability of date fruit seed biochar was compared with that of previous investigations, and sorption capacity (q_{max}) was used for comparison (Table 8). Different materials reflected differences in DR28 dye uptake efficiency under different operational conditions because of modifications to the surface area, porosity, and the presence of binding sites. The present study clearly showed that the sorption capacity of DFSB was better than that of other adsorbents; thus, DFSB can be used as a sustainable substitute for the sorption of DR28 dye. Further studies are needed for the application of date fruit seeds available at zero cost to enable its effective translation from the laboratory scale to real industrial effluent treatment.

Table 8. Adsorption (q_{max}) of DR28 dye with various sorbents.

Adsorbent Material	Experimental Conditions	q_{max} (mg g^{-1})	References
Activated charcoal	pH = 2, exposure time = 0.67 h, Dose = 1 g	0.93	Rehman et al. [61]
Raphanus sativus peel	pH = 3, exposure time = 0.33 h, Dose = 2 g	0.07	Rehman et al. [61]
Grewia asiatica leaves	pH = 7, exposure time = 0.5 h, Dose = 0.5 g	0.057	Rehman et al. [61]
Vermicompost-derived biochar	pH =7, exposure time = 2 h, Dose = 0.3 g	31	Yang et al. [62]
Cow dung biochar	pH = 7, exposure time = 84 h, Dose = 5 g	13	Khan et al. [77]
Rice husk biochar	pH = 7, exposure time = 84 h, Dose = 5 g	15.8	Khan et al. [77]
Pomegranate	pH = 7, exposure time = 0.5 h, Dose = 1 g	19.23	Ghaedi et al. [78]
Vaterite calcium carbonate	pH = 7, exposure time = 3 h, Dose = 0.2 mg	17	Chong et al. [79]
Molybdenum disulfide nanopowder	pH = 3, exposure time = 3 h, Dose = 0.1 g	81	Alarifi et al. [80]

Table 8. *Cont.*

Adsorbent Material	Experimental Conditions	q_{max} (mg g^{-1})	References
Eichhornia crassipes biomass	pH = 7, exposure time = 0.75 h, Dose = 0.125 g	14	Roy and Mondal [81]
Rabbit manure biochar	pH = 5, exposure time = 3.5 h, Dose = 0.15 g	28.4	Huang et al. [82]
Algal biochar	pH = 2, exposure time = 0.17 h, Dose = 0.2 g	51.3	Nautiyal et al. [60]
Date fruit seed biochar	pH = 3, exposure time = 4 h, Dose = 3 g	5.83	This study

4. Conclusions

The current investigation revealed that DFSB removed DR28 dye and can act as a sustainable alternative to other expensive methods. The appearance of different active sites on DFSB might be used in the adsorption of DR28 dye, as observed by the FTIR spectra. The sorption of DR28 dye followed the Langmuir rather than the Freundlich and Temkin models. The Langmuir adsorption isotherm model best represented the experimental points and reflected a maximum 5.83 mg/g adsorption capacity. The kinetics of sorption showed that the sorption rate was explained with a pseudo-second-order model. The exothermic nature of sorption was reflected by a negative value of ΔH^0. The thermodynamic variables showed that the sorption process was spontaneous and removed DR28 dye at a low temperature. The regenerated DFSB indicated favorable results for five succeeding cycles for the removal of DR28 dye. The DFSB-treated DR28 dye solution showed 83% pigeon pea seed germination and enhanced seedling growth. Therefore, DFSB can be utilized as a reliable, sustainable, cost-effective sorbent for DR28 dye elimination, and treated water can be used for irrigation purposes. In this way, the present study fulfills the objectives of the sustainable developmental goals for waste reduction and recycling to promote sustainability. However, detailed investigations are needed for the life cycle assessment of sorbents obtained after reutilization for up to five cycles, as they can be used in the preparation of value-added products, such as construction materials. Therefore, using biomass waste-based green adsorbents, we can promote the waste-to-wealth conversion strategy for environmental sustainability and a low-carbon circular economy, moving toward carbon neutrality.

References

1. Slama, H.B.; Chenari Bouket, A.; Pourhassan, Z.; Alenezi, F.N.; Silini, A.; Cherif-Silini, H.; Oszako, T.; Luptakova, L.; Golińska, P.; Belbahri, L. Diversity of synthetic dyes from textile industries, discharge impacts and treatment methods. *Appl. Sci.* **2021**, *11*, 6255. [CrossRef]

2. Enache, A.C.; Cojocaru, C.; Samoila, P.; Ciornea, V.; Apolzan, R.; Predeanu, G.; Harabagiu, V. Adsorption of brilliant green dye onto a mercerized biosorbent: Kinetic, thermodynamic, and molecular docking studies. *Molecules* **2023**, *28*, 4129. [CrossRef] [PubMed]

3. Daud, Z.; Detho, A.; Rosli, M.A.; Abubakar, M.H.; Samo, K.A.; Rais, N.F.M.; Halim, A.A.; Tajarudin, H.A. Ammoniacal nitrogen and COD removal from stabilized landfill leachate using granular activated carbon and green mussel (*Perna viridis*) shell powder as a composite adsorbent. *Desalination Water Treat* **2020**, *192*, 111–117. [CrossRef]

4. Ledakowicz, S.; Pazdzior, K. Recent achievements in dyes removal focused on advanced oxidation processes integrated with biological methods. *Molecules* **2021**, *26*, 870. [CrossRef] [PubMed]

5. Benkhaya, S.; Mrabet, S.; El Harfi, A. Classifications, properties, recent synthesis and applications of azo dyes. *Heliyon* **2020**, *6*, e03271. [CrossRef] [PubMed]

6. Parthasarathy, P.; Sajjad, S.; Saleem, J.; Alherbawi, M.; Mckay, G.A. Review of the removal of dyestuffs from effluents onto biochar. *Separations* **2022**, *9*, 139. [CrossRef]

7. Barathi, S.; Karthik, C.; Nadanasabapathi, S.; Padikasan, I.A. Biodegradation of textile dye reactive blue 160 by *Bacillus firmus* (Bacillaceae: Bacillales) and non-target toxicity screening of their degraded products. *Toxicol. Rep.* **2020**, *7*, 16–22. [CrossRef]

8. Nidheesh, P.V.; Divyapriya, G.; Titchou, F.E.; Hamdani, M. Treatment of textile wastewater by sulfate radical based advanced oxidation processes. *Sep. Purif. Technol.* **2022**, *293*, 121115. [CrossRef]

9. Han, Q.; Yang, Y.; Wang, R.; Zhang, K.; Liu, N.; Hong, M. Biochar derived from agricultural wastes as a means of facilitating the degradation of azo dyes by sulfides. *Catalysts* **2021**, *11*, 434. [CrossRef]

10. Sackey, E.A.; Song, Y.; Yu, Y.; Zhuang, H. Biochars derived from bamboo and rice straw for sorption of basic red dyes. *PLoS ONE* **2021**, *16*, e0254637. [CrossRef]

11. Sait, H.H.; Hussain, A.; Bassyouni, M.; Ali, I.; Kanthasamy, R.; Ayodele, B.V.; Elhenawy, Y. Anionic dye removal using a date palm seed-derived activated carbon/chitosan polymer microbead biocomposite. *Polymers* **2022**, *14*, 2503. [CrossRef] [PubMed]

12. Nindjio, G.F.K.; Tagne, R.F.T.; Jiokeng, S.L.Z.; Fotsop, C.G.; Bopda, A.; Doungmo, G.; Temgoua, R.C.T.; Doench, I.; Njoyim, E.T.; Tamo, A.K.; et al. Lignocellulosic-based materials from bean and pistachio pod wastes for dye-contaminated water treatment: Optimization and modeling of indigo carmine sorption. *Polymers* **2022**, *14*, 3776. [CrossRef] [PubMed]

13. Albahnasawi, A.; Yüksel, E.; Gürbulak, E.; Duyum, F. Fate of aromatic amines through decolorization of real textile wastewater under anoxic-aerobic membrane bioreactor. *J. Environ. Chem. Eng.* **2020**, *8*, 104226. [CrossRef]

14. Abd-Elhamid, A.I.; Emran, M.; El-Sadek, M.H.; El-Shanshory, A.A.; Soliman, H.M.; Akl, M.A.; Rashad, M. Enhanced removal of cationic dye by eco-friendly activated biochar derived from rice straw. *Appl. Water Sci.* **2020**, *10*, 1–11. [CrossRef]

15. Santoso, E.; Ediati, R.; Kusumawati, Y.; Bahruji, H.; Sulistiono, D.O.; Prasetyoko, D. Review on recent advances of carbon based adsorbent for methylene blue removal from waste water. *Mater. Today Chem.* **2020**, *16*, 100233. [CrossRef]

16. Vadivel, V.K.; Cikurel, H.; Mamane, H. Removal of indigo dye by $CaCO_3/Ca(OH)_2$ composites and resource recovery. *Ind. Eng. Chem. Res.* **2021**, *60*, 10312–10318. [CrossRef]

17. Alsukaibi, A.K. Various approaches for the detoxification of toxic dyes in wastewater. *Processes* **2022**, *10*, 1968. [CrossRef]

18. Xiang, H.; Min, X.; Tang, C.J.; Sillanpää, M.; Zhao, F. Recent advances in membrane filtration for heavy metal removal from wastewater: A mini review. *J. Water Process Eng.* **2022**, *49*, 103023. [CrossRef]

19. Zainudin, N.F.; Sam, S.T.; Wong, Y.S.; Ismail, H.; Walli, S.; Inoue, K.; Kawamura, G.; Tan, W.K. Degradation of diazo congo red dye by using synthesized poly-ferric-silicate-sulphate through co-polymerization process. *Polymers* **2023**, *15*, 237. [CrossRef]

20. Hamad, H.N.; Idrus, S. Recent developments in the application of bio-waste-derived adsorbents for the removal of methylene blue from wastewater: A review. *Polymers* **2022**, *14*, 783. [CrossRef]

21. Değermenci, G.D.; Değermenci, N.; Ayvaoğlu, V.; Durmaz, E.; Çakır, D.; Akan, E. Adsorption of reactive dyes on lignocellulosic waste; characterization, equilibrium, kinetic and thermodynamic studies. *J. Clean. Prod.* **2019**, *225*, 1220–1229. [CrossRef]

22. Mokhtar, N.; Johari, M.A.M.; Tajarudin, H.A.; AlGheethi, A.A.; AlgaifiA, H.A. Sustainable enhancement of bio-cement using immobilised *Bacillus sphaericus*: Optimization, microstructural properties, and techno-economic analysis for a cleaner production of bio-cementitious mortars. *J. Clean. Prod.* **2021**, *318*, 128470. [CrossRef]

23. Kaab, A.; Sharifi, M.; Mobli, H.; Nabavi-Pelesaraei, A.; Chau, K.W. Combined life cycle assessment and artificial intelligence for prediction of output energy and environmental impacts of sugarcane production. *Sci. Total Environ.* **2019**, *664*, 1005–1019. [CrossRef] [PubMed]

24. Goswami, L.; Kushwaha, A.; Kafle, S.R.; Kim, B.S. Surface modification of biochar for dye removal fromwastewater. *Catalysts* **2022**, *12*, 817. [CrossRef]

25. Kim, D.Y.; Jung, G.B. Effects of pyrolysis and ball-milling on the physicochemical and rhodamine b removal characteristics of rice-bran-derived biochar. *Appl. Sci.* **2023**, *13*, 4288. [CrossRef]

26. Kapoor, R.T.; Rafatullah, M.; Siddiqui, M.R.; Khan, M.A.; Sillanpää, M. Removal of reactive black 5 dye by banana peel biochar and evaluation of its phytotoxicity on tomato. *Sustainability* **2022**, *14*, 4176. [CrossRef]

27. Kapoor, R.T.; Rafatullah, M.; Aljuwayid, A.M.; Habila, M.A.; Wabaidur, S.M.; Alam, M. Removal of patent blue dye using *Ananas comosus*-derived biochar: Equilibrium, kinetics, and phytotoxicity studies. *Separations* **2022**, *9*, 426. [CrossRef]

28. Ying, Z.; Chen, X.; Li, H.; Liu, X.; Zhang, C.; Zhang, J.; Yi, G. Efficient adsorption of methylene blue by porous biochar derived from soybean dreg using a one-pot synthesis method. *Molecules* **2021**, *26*, 661. [CrossRef]

29. Kali, A.; Amar, A.; Loulidi, I.; Hadey, C.; Jabri, M.; Alrashdi, A.A.; Lgaz, H.; Sadoq, M.; El-Kordy, A.; Boukhlifi, F. Efficient adsorption removal of an anionic azo dye by lignocellulosicwaste material and sludge recycling into combustible briquettes. *Colloids Interfaces* **2022**, *6*, 22. [CrossRef]

30. Zeghioud, H.; Fryda, L.; Djelal, H.; Assadi, A.; Kane, A. A comprehensive review of biochar in removal of organic pollutants from wastewater: Characterization, toxicity, activation/functionalization and influencing treatment factors. *J. Water Process Eng.* **2022**, *47*, 102801. [CrossRef]

31. Ramos, R.; Abdelkader-Fernández, V.K.; Matos, R.; Peixoto, A.F.; Fernandes, D.M. Metal-supported biochar catalysts for sustainable biorefinery, electrocatalysis, and energy storage applications: A review. *Catalysts* **2022**, *12*, 207. [CrossRef]

32. Siddiqui, S.I.; Allehyani, E.S.; Al-Harbi, S.A.; Hasan, Z.; Abomuti, M.A.; Rajor, H.K.; Oh, S. Investigation of congo red toxicity towards different living organisms: A review. *Processes* **2023**, *11*, 807. [CrossRef]

33. Chawla, S.; Uppal, H.; Yadav, M.; Bahadur, N.; Singh, N. Zinc peroxide nanomaterial as an adsorbent for removal of congo red dye from waste water. *Ecotoxicol. Environ. Saf.* **2017**, *135*, 68–74. [CrossRef] [PubMed]

34. Hua, Z.; Pan, Y.; Hong, Q. Adsorption of congo red dye in water by orange peel biochar modified with CTAB. *RSC Adv.* **2023**, *13*, 12502–12508. [CrossRef] [PubMed]

35. Naseem, K.; Farooqi, Z.H.; Begum, R.; Irfan, A. Removal of congo red dye from aqueous medium by its catalytic reduction using sodium borohydride in the presence of various inorganic nano-catalysts: A review. *J. Clean. Prod.* **2018**, *187*, 296–307. [CrossRef]

36. Echegaray, N.; Gullón, B.; Pateiro, M.; Amarowicz, R.; Misihairabgwi, J.M.; Lorenzo, J.M. Date fruit and its by-products as promising source of bioactive components: A review. *Food Rev. Int.* **2021**, *39*, 1411–1432. [CrossRef]

37. Fernández-López, J.; Viuda-Martos, M.; Sayas-Barberá, E.; Navarro-Rodríguez de Vera, C.; Pérez-Álvarez, J.Á. Biological, nutritive, functional and healthy potential of date palm fruit (*Phoenix dactylifera*): Current research and future prospects. *Agronomy* **2022**, *12*, 876. [CrossRef]

38. Rybicka, I.; Kiewlicz, J.; Kowalczewski, P.L.; Gliszczynska-'Swigło, A. Selected dried fruits as a source of nutrients. *Eur. Food Res. Technol.* **2021**, *247*, 2409–2419. [CrossRef]

39. Al-Shankiti, A.; Gill, S. Biochar from date palm and *Conocarpus* waste for improvement of soil quality and biomass production. *Biosalinity New* **2014**, *15*, 8–9.

40. Jeevarathinam, G.; Chelladurai, V. Pigeon pea. In *Pulses*; Springer: Berlin/Heidelberg, Germany, 2020; pp. 275–296.

41. Gargi, B.; Semwal, P.; Jameel Pasha, S.B.; Singh, P.; Painuli, S.; Thapliyal, A.; Cruz-Martins, N. Revisiting the nutritional, chemical and biological potential of *Cajanus cajan* (L.) Millsp. *Molecules* **2022**, *27*, 6877. [CrossRef]

42. Cebrian, G.; Condon, S.; Manas, P. Physiology of the inactivation of vegetative bacteria by thermal treatments: Mode of action, influence of environmental factors and inactivation kinetics. *Foods* **2017**, *6*, 107. [CrossRef] [PubMed]

43. Rivera-Utrilla, J.; Bautista-Toledo, I.; Ferro-García, M.A.; Moreno-Castilla, C. Activated carbon surface modifications by adsorption of bacteria and their effect on aqueous lead adsorption. *J. Chem. Technol. Biotechnol.* **2001**, *76*, 1209–1215. [CrossRef]

44. Bharathi, K.S.; Ramesh, S.P.T. Fixed-bed column studies on biosorption of crystal violet from aqueous solution by *Citrullus lanatus* rind and *Cyperus rotundus*. *Appl. Water Sci.* **2013**, *3*, 673–687. [CrossRef]

45. Ng, J.C.Y.; Cheung, W.H.; McKay, G. Equilibrium studies of the sorption of Cu (II) ions onto chitosan. *J. Colloid Interface Sci.* **2002**, *255*, 64–74. [CrossRef] [PubMed]

46. Temkin, M.I.; Pyzhev, V. Kinetics of ammonia synthesis on promoted iron catalyst. *Acta Phys. Chim. USSR* **1940**, *12*, 327–356.

47. Lagergren, S. About the theory of so-called adsorption of soluble substances. *K. Sven. Vetenskapsakademiens Handl.* **1898**, *24*, 1–39.

48. Ho, Y.S.; Mckay, G. Pseudo-second-order model for sorption processes. *Process Biochem.* **1999**, *34*, 451–465. [CrossRef]

49. Weber, W.J.; Morris, J.C. Kinetics of adsorption on carbon from solution. *J. Sanit. Eng. Div.* **1963**, *89*, 31–60. [CrossRef]

50. Kapoor, R.T.; Selvaraju Sivamani, S. Exploring the potential of *Eucalyptus citriodora* biochar against direct red 31 dye and its phytotoxicity assessment. *Biomass Convers. Biorefin.* **2021**, *13*, 8011–8022. [CrossRef]

51. ISTA. *International Rules for Seed Testing*; International Seed Testing Association, ISTA Secretariat: Bassersdorf, Switzerland, 2008.

52. Lichtenthaler, H.K. Chlorophylls and carotenoids: Pigments of photosynthetic biomembranes. *Methods Enzymol.* **1987**, *148*, 350–382.

53. Hedge, J.E.; Hofreiter, B.T. *Carbohydrate Chemistry 17*; Whistler, R.L., Be Miller, J.N., Eds.; Academic Press: New York, NY, USA, 1962; pp. 17–22.

54. Bates, L.S.; Waldren, R.P.; Teare, I.D. Rapid determination of free proline for water-stress studies. *Plant Soil* **1973**, *39*, 205–207. [CrossRef]

55. Lowry, O.H.; Rosebrough, N.J.; Farr, A.L.; Randall, R.J. Protein measurement with the folin phenol reagent. *J. Biol. Chem.* **1951**, *193*, 265–275. [CrossRef] [PubMed]

56. Kushwaha, A.; Rani, R.; Kumar, S.; Thomas, T.; David, A.A.; Ahmed, M. A new insight to adsorption and accumulation of high lead concentration by exopolymer and whole cells of lead-resistant bacterium *Acinetobacter junii* L. Pb1 isolated from coal mine dump. *Environ. Sci. Pollut. Res.* **2017**, *24*, 10652–10661. [CrossRef] [PubMed]

57. Wisniewska, M.; Chibowski, S.; Wawrzkiewicz, M.; Onyszko, M.; Bogatyrov, V.C.I. Basic Red 46 removal from sewage by carbon and silica based composite: Equilibrium, kinetic and electrokinetic studies. *Molecules* **2022**, *27*, 1043. [CrossRef]

58. Chanzu, H.A.; Onyari, J.M.; Shiundu, P.M. Brewers' spent grain in adsorption of aqueous congo red and malachite green dyes: Batch and continuous flow systems. *J. Hazard. Mater.* **2019**, *380*, 120897. [CrossRef] [PubMed]

59. Dai, H.; Xu, S.; Chen, J.; Miao, X.; Zhu, J. Oxalate enhanced degradation of orange II in heterogeneous UV-fenton system catalyzed by $Fe_3O_4@\Gamma\text{-}Fe_2O_3$ composite. *Chemosphere* **2018**, *199*, 147–153. [PubMed]

60. Nautiyal, P.; Subramanian, K.A.; Dastidar, M.G. Adsorptive removal of dye using biochar derived from residual algae after in-situ transesterification: Alternate use of waste of biodiesel industry. *J. Environ. Manag.* **2016**, *182*, 187–197.

61. Rehman, R.; Murtaza, S.; Zaman, W.; Shafique, U. Comparative removal of congo red dye from water by adsorption on *Grewia asiatica* leaves, *Raphanus sativus* peels and activated charcoal. *J. Chem. Soc. Pak.* **2012**, *34*, 112.

62. Yang, G.; Wu, L.; Xian, Q.; Shen, F.; Wu, J.; Zhang, Y. Removal of congo red and methylene blue from aqueous solutions by vermicompost-derived biochars. *PLoS ONE* **2016**, *11*, e0154562. [CrossRef]

63. Salameh, Y.; Albadarin, A.B.; Allen, S.; Walker, G.; Ahmad, M.N.M. Arsenic (III, V) adsorption onto charred dolomite: Charring optimization and batch studies. *Chem. Eng. J.* **2015**, *259*, 663–671. [CrossRef]

64. Jamali-Behnam, F.; Najafpoor, A.A.; Davoudi, M.; Rohani-Bastami, T.; Alidadi, H.; Esmaily, H.; Dolatabadi, M. Adsorptive removal of arsenic from aqueous solutions using magnetite nanoparticles and silica-coated magnetite nanoparticles. *Environ. Prog. Sustain. Energy* **2018**, *37*, 951–960. [CrossRef]

65. Joardder, M.U.H.; Uddin, M.S.; Islam, M.N. The utilization of waste date seed as bio-oil and activated carbon by pyrolysis process. *Adv. Mech. Eng.* **2012**, *4*, 316806. [CrossRef]

66. Enaime, G.; Baçaoui, A.; Yaacoubi, A.; Lübken, M. Biochar for wastewater treatment-conversion technologies and applications. *Appl. Sci.* **2020**, *10*, 3492. [CrossRef]

67. Kaya, N.; Yıldız, Z.; Ceylan, S. Preparation and characterisation of biochar from hazelnut shell and its adsorption properties for methylene blue dye. *Politek. Derg.* **2018**, *21*, 765–776. [CrossRef]

68. Neupane, S.; Ramesh, S.T.; Gandhimathi, R.; Nidheesh, P.V. Pineapple leaf (*Ananas comosus*) powder as a biosorbent for the removal of crystal violet from aqueous solution. *Desalination Water Treat.* **2015**, *54*, 2041–2054. [CrossRef]

69. Ambaye, T.G.; Vaccari, M.; van Hullebusch, E.D.; Amrane, A.; Rtimi, S. Mechanisms and adsorption capacities of biochar for the removal of organic and inorganic pollutants from industrial wastewater. *Int. J. Environ. Sci. Technol.* **2021**, *18*, 3273–3294.

70. Wu, K.; Pan, X.; Zhang, J.; Zhang, X.; Salah Zene, A.; Tian, Y. Biosorption of congo red from aqueous solutions based on self-immobilized mycelial pellets: Kinetics, isotherms, and thermodynamic studies. *ACS Omega* **2020**, *5*, 24601–24612. [PubMed]

71. Bao, Y.; Zhang, G. study of adsorption characteristics of methylene blue onto activated carbon made by *Salix psammophila*. *Energy Procedia* **2012**, *16*, 1141–1146. [CrossRef]

72. Bashanaini, M.S.; Al-Douh, M.H.; Al-Ameri, H.S. Removal of malachite green dye from aqueous solution by adsorption using modified and unmodified local agriculture waste. *Sci. J. Anal. Chem.* **2019**, *7*, 42–56.

73. Rubangakene, N.O.; Elwardany, A.; Fujii, M.; Sekiguchi, H.; Elkady, M.; Shokry, H. Biosorption of congo red dye from aqueous solutions using pristine biochar and ZnO biochar from green pea peels. *Chem. Eng. Res. Des.* **2023**, *189*, 636–651.

74. Duarte Neto, J.F.; Pereira, I.D.S.; Da Silva, V.C.; Ferreira, H.C.; Neves, D.G.A.; Menezes, R.R. Study of equilibrium and kinetic adsorption of rhodamine B onto purified bentonite clays. *Ceramica* **2018**, *64*, 598–607. [CrossRef]

75. Perez-Calderon, J.; Santos, M.V.; Zaritzky, N. Reactive red 195 dye removal using chitosan coacervated particles as bio-sorbent: Analysis of kinetics, equilibrium and adsorption mechanisms. *J. Environ. Chem. Eng.* **2018**, *6*, 6749–6760. [CrossRef]

76. Karthick, K.; Namasivayam, C.; Pragasam, L.A. Removal of direct red 12B from aqueous medium by $ZnCl_2$ activated *Jatropha* husk carbon: Adsorption dynamics and equilibrium studies. *Ind. J. Chem. Technol.* **2017**, *24*, 73–81.

77. Khan, N.; Chowdhary, P.; Ahmad, A.; Giri, B.S.; Chaturvedi, P. Hydrothermal liquefaction of rice husk and cow dung in mixed-bed-rotating pyrolyzer and application of biochar for dye removal. *Bioresour. Technol.* **2020**, *309*, 123294. [CrossRef] [PubMed]

78. Ghaedi, M.; Tavallali, H.; Sharifi, M.; Kokhdan, S.N.; Asghari, A. Preparation of low cost activated carbon from *Myrtus communis* and pomegranate and their efficient application for removal of congo red from aqueous solution. *Spectrochim. Acta A Mol. Biomol. Spectrosc.* **2012**, *86*, 107–114. [CrossRef] [PubMed]

79. Chong, K.Y.; Chia, C.H.; Zakaria, S.; Sajab, M.S. Vaterite calcium carbonate for the adsorption of congo red from aqueous solutions. *J. Environ. Chem. Eng.* **2014**, *2*, 2156–2161.

80. Alarifi, I.M.; Al-ghamdi, Y.O.; Darwesh, R.; Omaish, M.; Kashif, M. Properties and application of MoS_2 nanopowder: Characterization, congo red dye adsorption, and optimization. *J. Mater. Res. Technol.* **2021**, *13*, 1169–1180. [CrossRef]

81. Roy, T.K.; Mondal, N.K. Biosorption of congo red from aqueous solution onto burned root of *Eichhornia crassipes* biomass. *Appl. Water Sci.* **2017**, *7*, 1841–1854. [CrossRef]

82. Huang, W.; Zhang, M.; Wang, Y.; Chen, J.; Zhang, J. Biochars prepared from rabbit manure for the adsorption of rhodamine B and congo red: Characterisation, kinetics, isotherms and thermodynamic studies. *Water Sci. Technol.* **2020**, *81*, 436–444. [CrossRef]